

# Quantitative High-Speed Imaging of Entire Developing Embryos with Simultaneous Multi-View Light Sheet Microscopy

Raju Tomer, Khaled Khairy, Fernando Amat and Philipp J. Keller\*

*Howard Hughes Medical Institute, Janelia Farm Research Campus*

\*Correspondence: [kellerp@janelia.hhmi.org](mailto:kellerp@janelia.hhmi.org)

## Supplementary Information

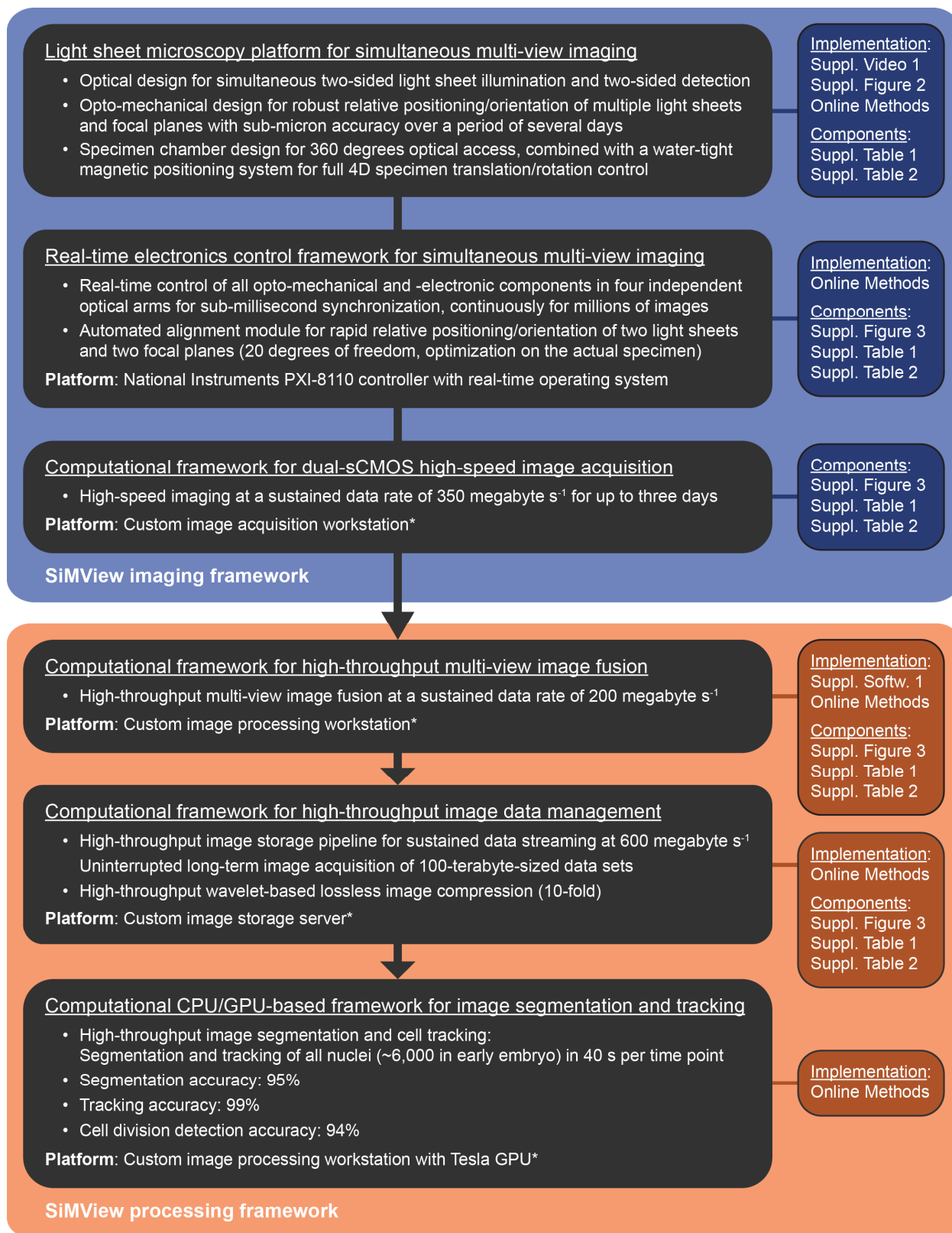
### Supplementary Figures

<b>Supplementary Figure 1</b>	Technology framework for simultaneous multi-view imaging
<b>Supplementary Figure 2</b>	Optical implementation of the SiMView imaging platform
<b>Supplementary Figure 3</b>	SiMView real-time electronics and computational hardware
<b>Supplementary Figure 4</b>	Point-spread-functions in one- and two-photon SiMView
<b>Supplementary Figure 5</b>	Spatio-temporal artifacts in sequential multi-view imaging
<b>Supplementary Figure 6</b>	Quantifying <i>Drosophila</i> nuclei dynamics in the syncytial blastoderm
<b>Supplementary Figure 7</b>	Simultaneous multi-view imaging of <i>Drosophila</i> embryogenesis
<b>Supplementary Figure 8</b>	Post-acquisition larval hatching in sequential multi-view imaging
<b>Supplementary Figure 9</b>	Manual cell tracking in the retracting germ band
<b>Supplementary Figure 10</b>	Reconstruction of neuroblast and epidermoblast lineages
<b>Supplementary Figure 11</b>	Time-course of <i>C155-GAL4,UAS-mCD8::eGFP</i> signal intensity
<b>Supplementary Figure 12</b>	SiMView optical slices of the <i>Drosophila</i> VNC and brain lobes

### Supplementary Tables

<b>Supplementary Table 1</b>	Components of the one-photon SiMView light sheet microscope
<b>Supplementary Table 2</b>	Components of the two-photon SiMView light sheet microscope
<b>Supplementary Table 3</b>	Specifications of simultaneous multi-view imaging experiments

## Supplementary Figure 1 | Technology framework for simultaneous multi-view imaging

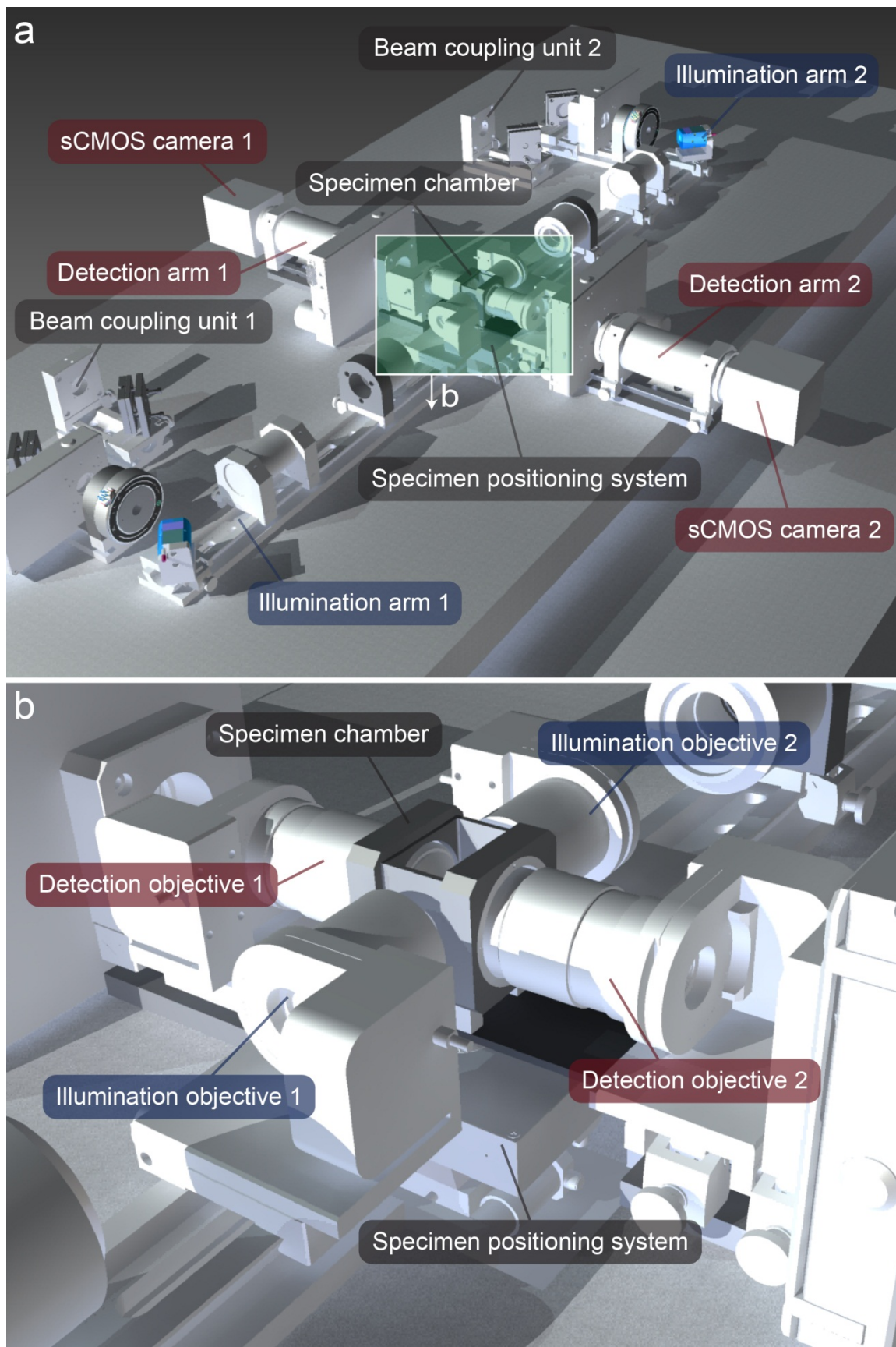


## **Supplementary Figure 1** | Technology framework for simultaneous multi-view imaging

The SiMView framework for simultaneous multi-view imaging consists of a light sheet microscopy platform with four independent optical arms, a real-time electronics control framework and three computational modules for dual-sCMOS high-speed image acquisition, high-throughput content-based multi-view image fusion and high-throughput image data management. A fourth post-processing pipeline performs fast and accurate image segmentation and cell tracking in SiMView live recordings of nuclei-labeled specimens.

This figure provides an overview of the key capabilities and functions of the six core modules, which are described in more detail in the **Online Methods**. The opto-mechanical components, electronics and computational hardware (marked with asterisks) are described in **Supplementary Figs. 2 and 3, Supplementary Tables 1 and 2** and in the **Online Methods**. Core modules of the computational framework for high-throughput multi-view image registration and image fusion are provided as **Supplementary Software**.

Supplementary Figure 2 | Optical implementation of the SiMView imaging platform

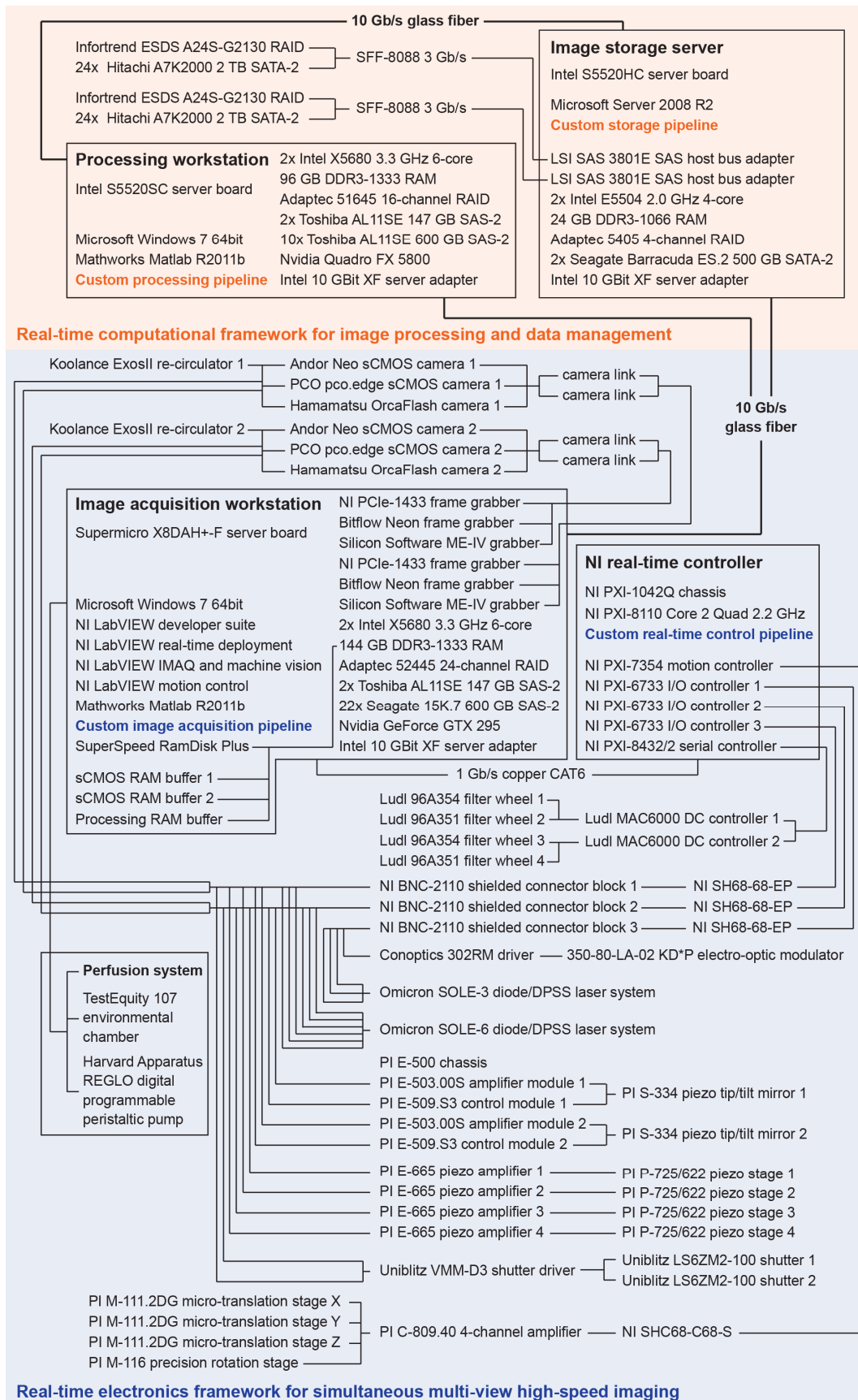


## Supplementary Figure 2 | Optical implementation of the SiMView imaging platform

(a) Computer model of the opto-mechanical implementation of the light sheet microscope for simultaneous multi-view imaging. The opto-mechanical modules of the instrument consist of two illumination arms for fluorescence excitation with scanned light sheets (blue), two fluorescence detection arms equipped with sCMOS cameras (red) as well as beam-coupling modules, specimen chamber and the specimen positioning system (grey). Each illumination sub-system comprises the following elements (listed according to appearance along the beam path, from beam coupling unit to specimen chamber): custom collimator module, mirror pair, illumination filter wheel, laser shutter, piezo tip/tilt mirror, f-theta lens, tube lens and piezo-mounted illumination objective. Each detection sub-system comprises the following elements (listed according to appearance along beam path from specimen chamber to detector): piezo-mounted detection objective, detection filter wheel, tube lens, tube system, sCMOS camera. Detailed information on all of the microscope's hardware components, including optics, mechanical parts, electronics and computer hardware, are provided in **Supplementary Tables 1 and 2**.

(b) Enlarged view of the central part of the microscope, where the four optical arms for simultaneous multi-view imaging meet at the specimen chamber. The specimen positioning system is located underneath the specimen chamber, which provides three essential advantages: full access to the specimen chamber from the top, sufficient space for opto-mechanical components in the four-arm arrangement surrounding the sample chamber, and mechanical specimen support by an upright specimen holder. The latter feature is required for specimen embedding in ultra-low concentration agarose gels for physiological long-term imaging experiments.

# Supplementary Figure 3 | SiMView real-time electronics and computational hardware

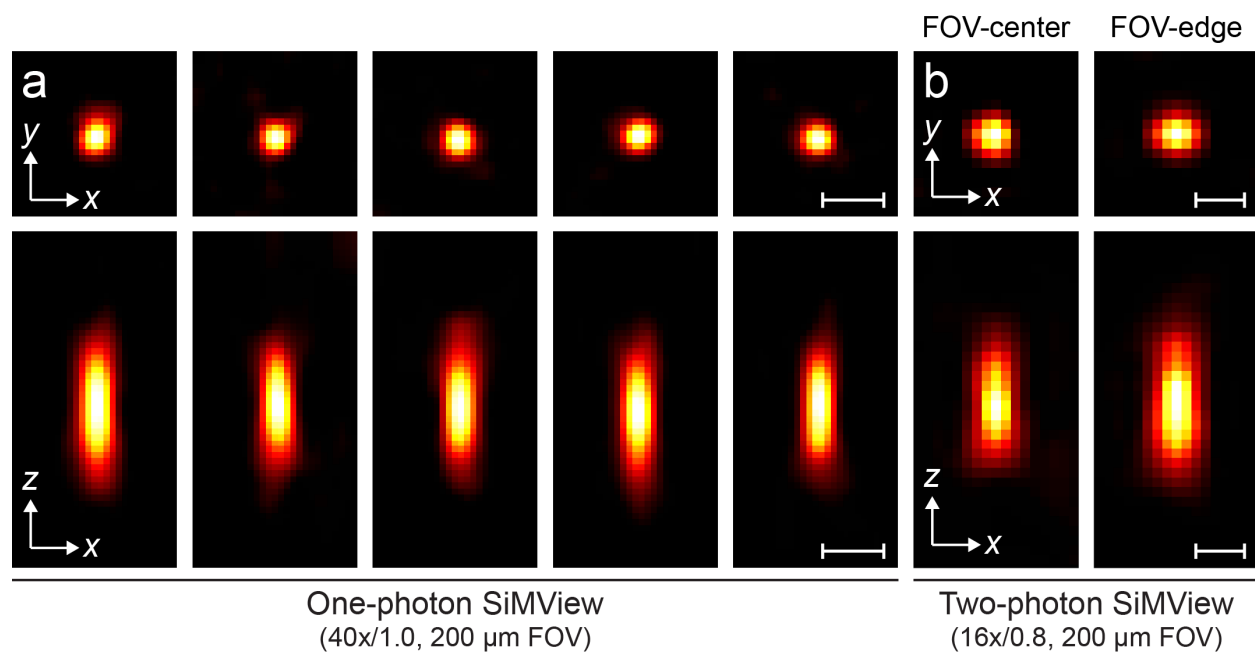


### **Supplementary Figure 3** | SiMView real-time electronics and computational hardware

This diagram shows the real-time electronics framework for precise control and relative timing of all opto-mechanical components of the SiMView imaging platform, as well as the integrated computational hardware for high-speed image acquisition and high-throughput multi-view image registration, image fusion, wavelet compression and image data management. Custom LabVIEW software communicates the process workflow to the NI real-time controller and coordinates data streaming on the image acquisition workstation. Custom Matlab software performs high-throughput image analysis on the processing workstation and manages the data stream to the storage server. Core modules of the high-throughput content-based multi-view image registration and image fusion pipeline are provided as **Supplementary Software**.

Optionally, an additional image processing workstation with a Tesla GPU (Nvidia Corporation) is integrated in the framework to enable high-throughput image segmentation and cell tracking using a custom image processing pipeline (see **Online Methods**).

Supplementary Figure 4 | Point-spread-functions in one- and two-photon SiMView



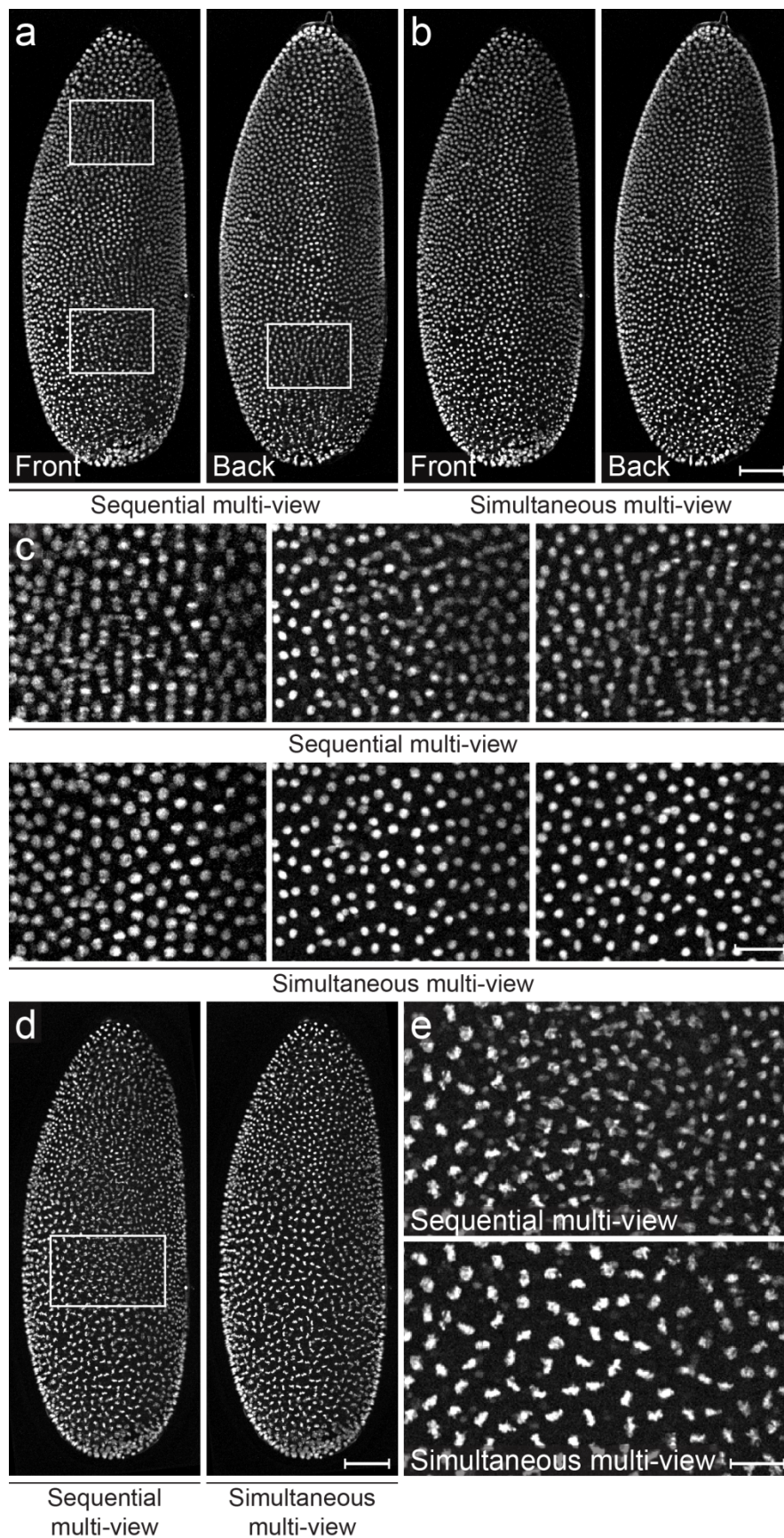
## Supplementary Figure 4 | Point-spread-functions in one- and two-photon SiMView

(a) Representative lateral (x,y) and axial (x,z) views of 50-nm-sized fluorescent beads recorded with the one-photon light sheet microscope for simultaneous multi-view imaging (one-photon SiMView). The microscope was equipped with 40x Carl Zeiss Plan-Apochromat water-dipping detection objectives (NA = 1.0), representing the optical configuration in recordings shown in **Supplementary Videos 16-20**. Average FWHM values resulted as  $0.399 \pm 0.025$   $\mu\text{m}$  laterally, and  $1.59 \pm 0.13$   $\mu\text{m}$  axially (mean  $\pm$  s.d.,  $n = 5$ ). A false color look-up-table was used to enhance visualization.

(b) Representative lateral (x,y) and axial (x,z) views of 50-nm-sized fluorescent beads recorded with the two-photon light sheet microscope for simultaneous multi-view imaging (two-photon SiMView). The microscope was equipped with 16x Nikon water-dipping detection objectives (NA = 0.8), representing the optical configuration in recordings shown in **Supplementary Videos 4-6**. Average FWHM values in the center of the field-of-view (FOV) resulted as  $0.603 \pm 0.086$   $\mu\text{m}$  laterally, and  $1.87 \pm 0.14$   $\mu\text{m}$  axially (mean  $\pm$  s.d.,  $n = 8$ ). Average FWHM values at the edge of the field-of-view (FOV) resulted as  $0.640 \pm 0.026$   $\mu\text{m}$  laterally, and  $2.29 \pm 0.06$   $\mu\text{m}$  axially (mean  $\pm$  s.d.,  $n = 2$ ). Note that lateral FWHM values are larger than in (a) owing to the lower sampling (and thus lower effective imaging resolution) obtained with the 16x detection objective. A false color look-up-table was used to enhance visualization.

Scale bars, 1  $\mu\text{m}$ .

Supplementary Figure 5 | Spatio-temporal artifacts in sequential multi-view imaging



## Supplementary Figure 5 | Spatio-temporal artifacts in sequential multi-view imaging

(a) Maximum-intensity projections of the front and back halves of a fused sequential four-view light sheet microscopy recording of a stage 4 *Drosophila* embryo just after the 13<sup>th</sup> mitotic cycle. To obtain the sequential multi-view panels, image fusion was performed on a subset of the simultaneous multi-view data set, corresponding to a 105 seconds delay between the first and last views.

(b) Corresponding projections of the fused simultaneous four-view light sheet microscopy recording of the same embryo at the same time point.

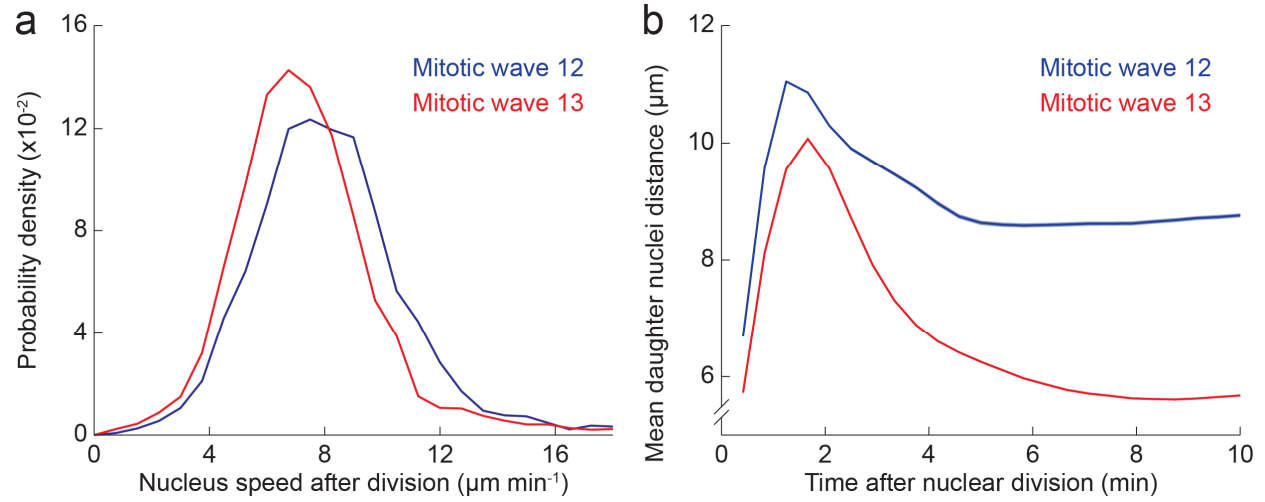
(c) Enlarged views of the regions indicated by white rectangles in (a). Shape information and temporal patterns are distorted in the sequential multi-view recording. Moreover, nuclei undergoing division are often accompanied by ghost images in the sequential multi-view recording.

(d) Maximum-intensity projections of the front half of a sequential (left) and a simultaneous (right) multi-view recording of the same embryo as in (a) during the 13<sup>th</sup> mitotic cycle. The delay between the first and last views in the sequential multi-view recording is 105 seconds.

(e) Enlarged views of the region indicated by a white rectangle in (d). In the sequential multi-view recording, nuclei appear in duplicates (or triplicates, if the nucleus is undergoing a division), which represent the same nucleus at different locations and in different mitotic states.

Scale bars, 50  $\mu\text{m}$  (a,b,d), 20  $\mu\text{m}$  (c,e).

Supplementary Figure 6 | Quantifying *Drosophila* nuclei dynamics in the syncytial blastoderm



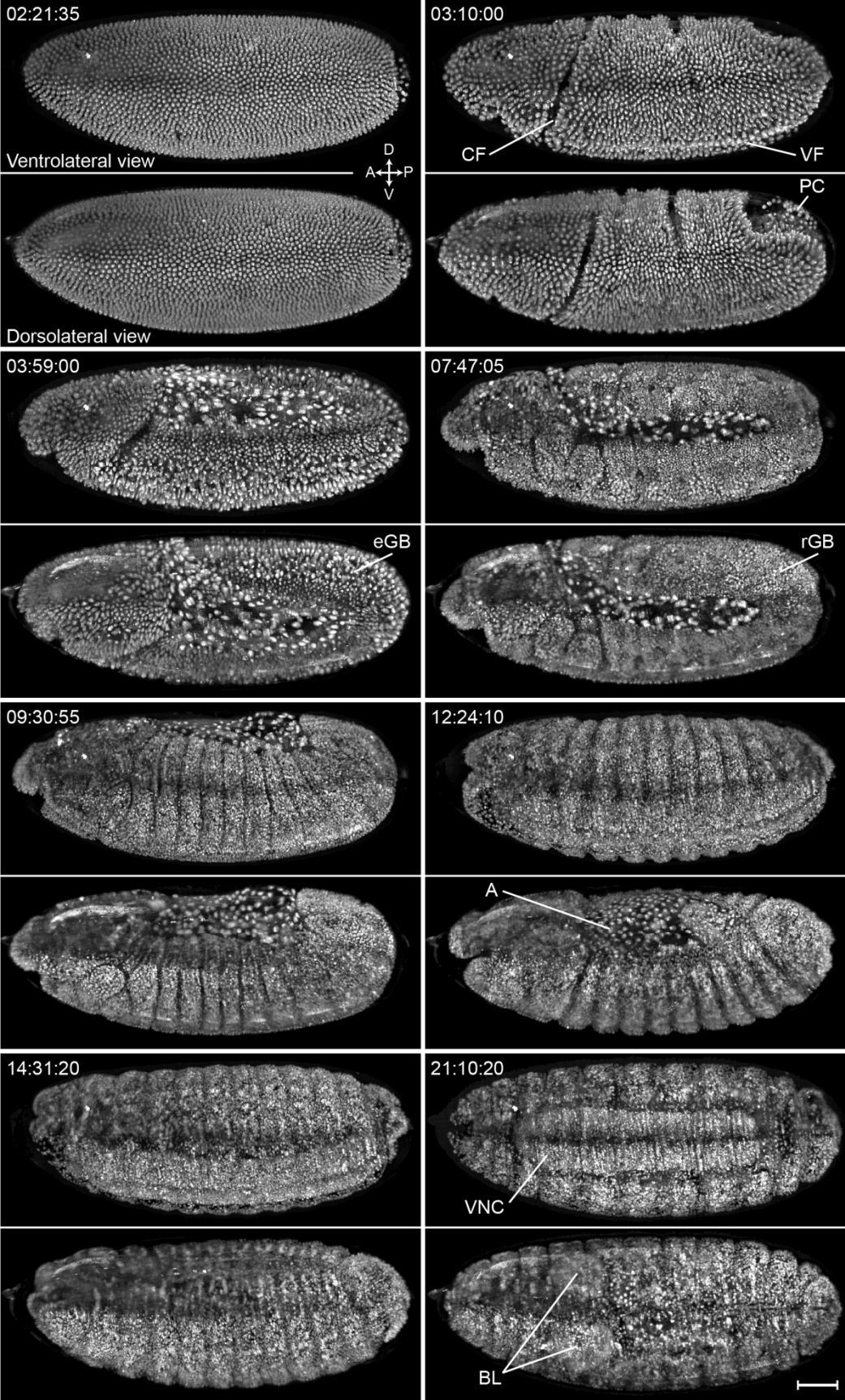
## Supplementary Figure 6 | Quantifying *Drosophila* nuclei dynamics in the syncytial blastoderm

Quantitative analysis of the 12<sup>th</sup> and 13<sup>th</sup> mitotic waves performed on the segmentation and tracking results shown in **Supplementary Video 8**. All statistics were obtained with Huber robust estimator (implemented and described in the Matlab function *robustfit*) in order to avoid bias from outliers arising from tracking inaccuracies as specified in the methods section “*Quantitative Estimation of Segmentation and Tracking Accuracy*”.

(a) Distribution of nuclei speeds directly after nuclear division. Mean and standard deviation are  $8.12 \pm 2.59 \mu\text{m min}^{-1}$  ( $n = 2,798$ ) for mitotic wave 12 and  $7.21 \pm 2.21 \mu\text{m min}^{-1}$  ( $n = 4,852$ ) for mitotic wave 13. These distributions represent the statistics used to obtain the values at  $t = 0.42$  min (global maxima) in **Fig. 5d**.

(b) Average distance between daughter nuclei from the same mother nucleus as a function of time  $t$  after nuclear division. As in **Fig. 5d**, the small standard error arises from the large sample size of  $\sim 2,500$ - $5,000$  samples per time point. The average distance between daughter nuclei reaches a maximum of  $11.05 \mu\text{m}$  at  $t = 1.25$  min after division for mitotic wave 12 and  $10.07 \mu\text{m}$  at  $t = 1.67$  min after division for mitotic wave 13, which is almost two-fold higher than the global average nearest neighbor distance of post-mitotic nuclei in the embryo shown in **Fig. 5e**. Subsequently, 10 minutes after division, the average distance between daughter nuclei relaxes to  $8.76 \mu\text{m}$  for mitotic wave 12 and to  $5.68 \mu\text{m}$  for mitotic wave 13, owing to the almost two-fold increase in nuclei count by the end of each mitotic wave.

Supplementary Figure 7 | Simultaneous multi-view imaging of *Drosophila* embryogenesis



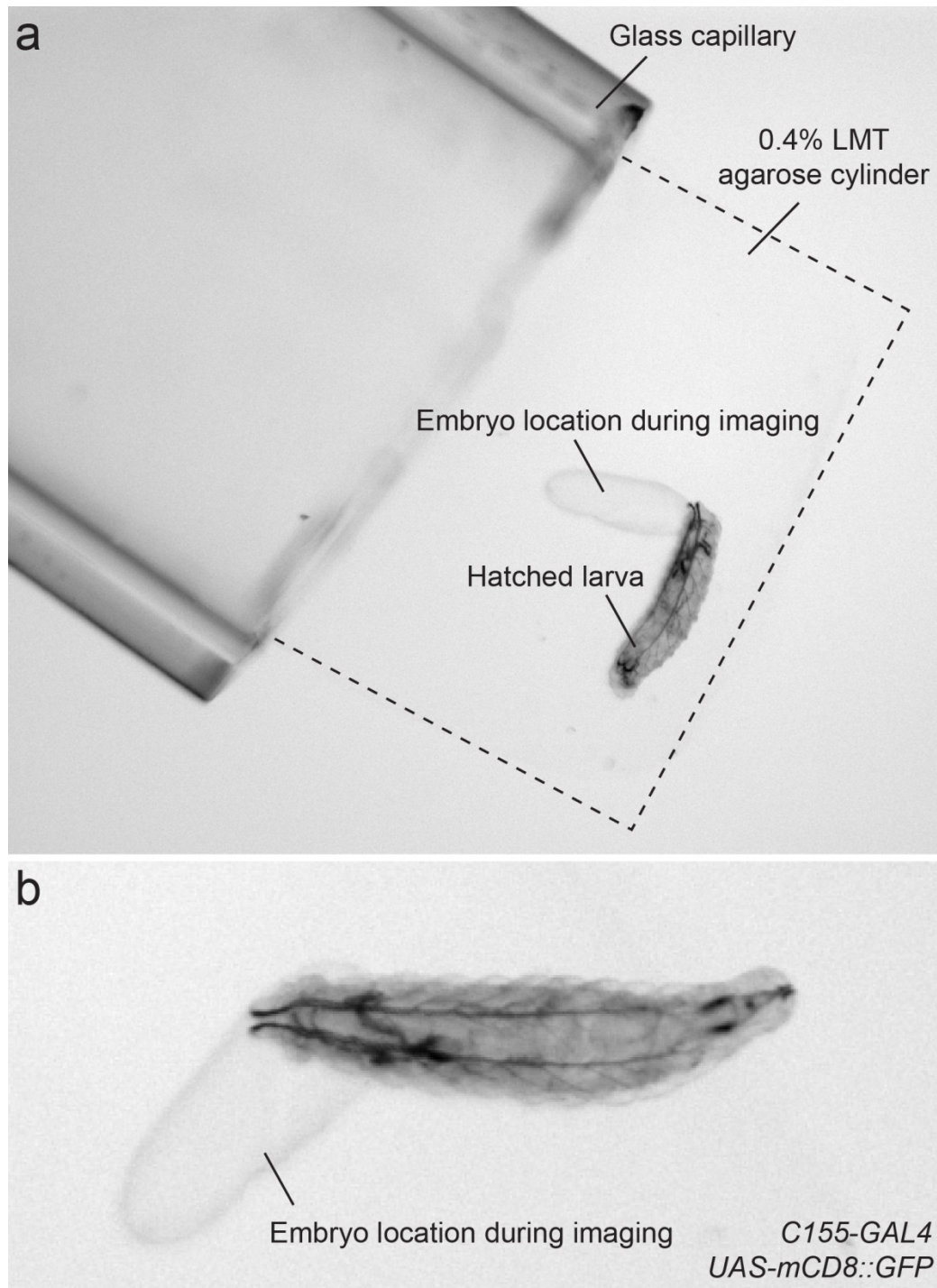
## Supplementary Figure 7 | Simultaneous multi-view imaging of *Drosophila* embryogenesis

Maximum-intensity projections of image stacks from a one-photon SiMView time-lapse recording of *Drosophila* embryonic development. Separate background-corrected maximum-intensity projections of the first and second halves of the fused three-dimensional image stacks are shown for eight time points, providing dorsolateral and ventrolateral views of the developing embryo. Owing to the activation of the embryonic muscular system towards the end of the recording, fast contractions are constantly reorienting the entire embryo (such as in the last panel, where the embryo is turned by approximately 90 degrees). Simultaneous multi-view imaging allows following development even through this technically particularly challenging period. The entire embryo was recorded in 35-second intervals over a period of 19.5 hours, using an image acquisition period of 15 seconds per time point. The complete recording comprises one million images (10 terabytes) for ~2,000 time points recorded from 2 to 21.5 hours post fertilization (**Supplementary Video 3**). A second recording of a different embryo from 3 to 18.5 hours post fertilization is provided as well (**Supplementary Video 2**).

PC = pole cells, VF = ventral furrow, eGB/rGB = extending/retracting germ band, CF = cephalic furrow, A = amnioserosa, VNC = ventral nerve cord, BL = brain lobes.

Scale bar, 50  $\mu\text{m}$ .

**Supplementary Figure 8** | Post-acquisition larval hatching in simultaneous multi-view imaging

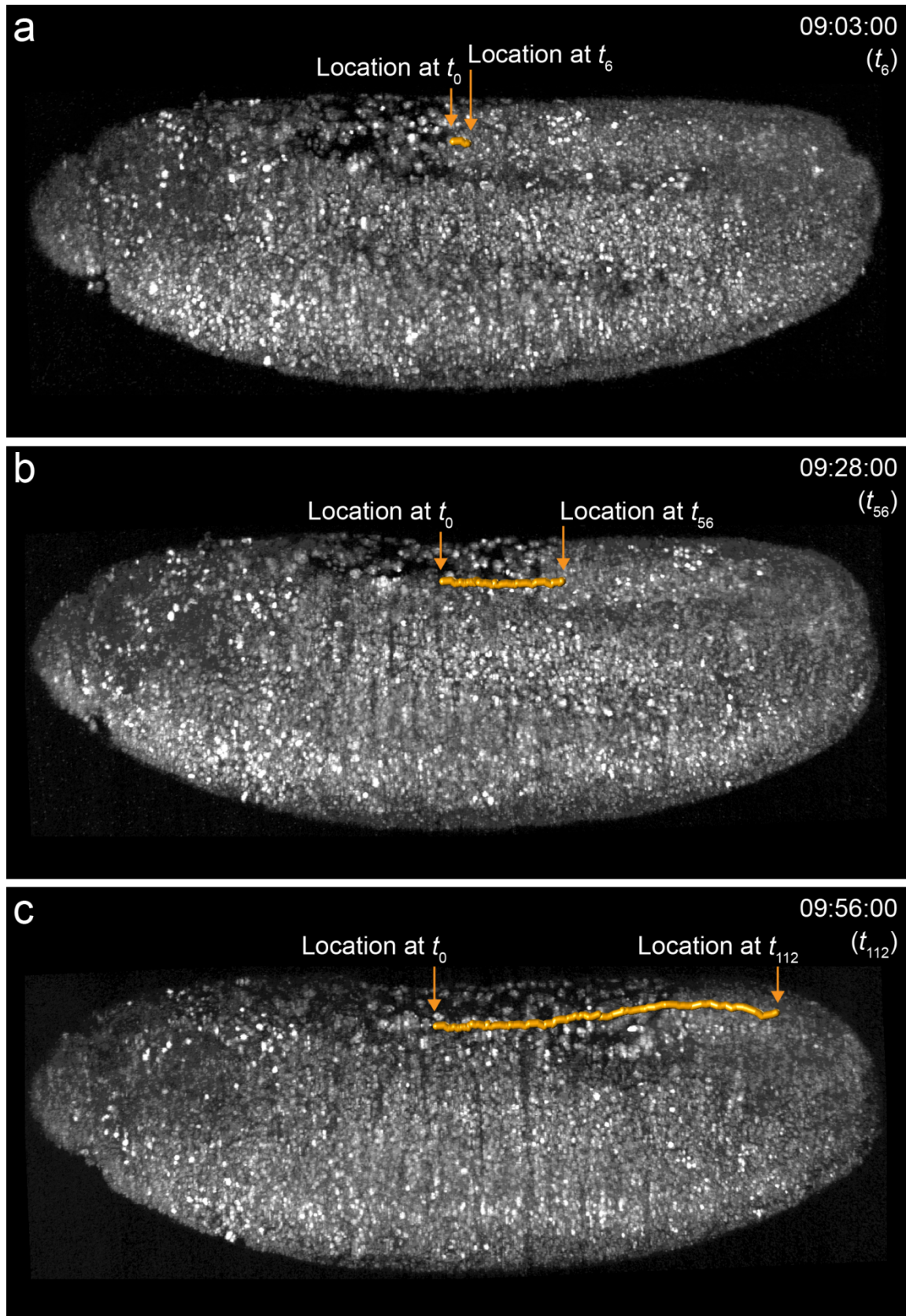


**Supplementary Figure 8** | Post-acquisition larval hatching in simultaneous multi-view imaging

(a) Image of the sample cylinder showing the hatched larva after long-term high-speed image acquisition of a developing embryo with the light sheet microscope. An ellipsoidal-shaped hollow space is visible in the 0.4% low-melting-temperature (LMT) agarose cylinder protruding from the glass capillary and indicates the previous location of the embryo during image acquisition. The larva shown here hatched from the embryo recorded in **Supplementary Video 12**. A short time sequence of the behaving larva is provided in **Supplementary Video 7**.

(b) Enlarged view of the hatched larva after time-lapse imaging of the *CI55-GAL4,UAS-mCD8::GFP* embryo in **Supplementary Video 12**.

Supplementary Figure 9 | Manual cell tracking in the retracting germ band



## Supplementary Figure 9 | Manual cell tracking in the retracting germ band

Manual tracking was performed for cells in a non-superficial layer of the retracting germ band, confirming that SiMView recordings also provide the spatio-temporal resolution required for quantitative analyses of cellular dynamics in late embryonic stages.

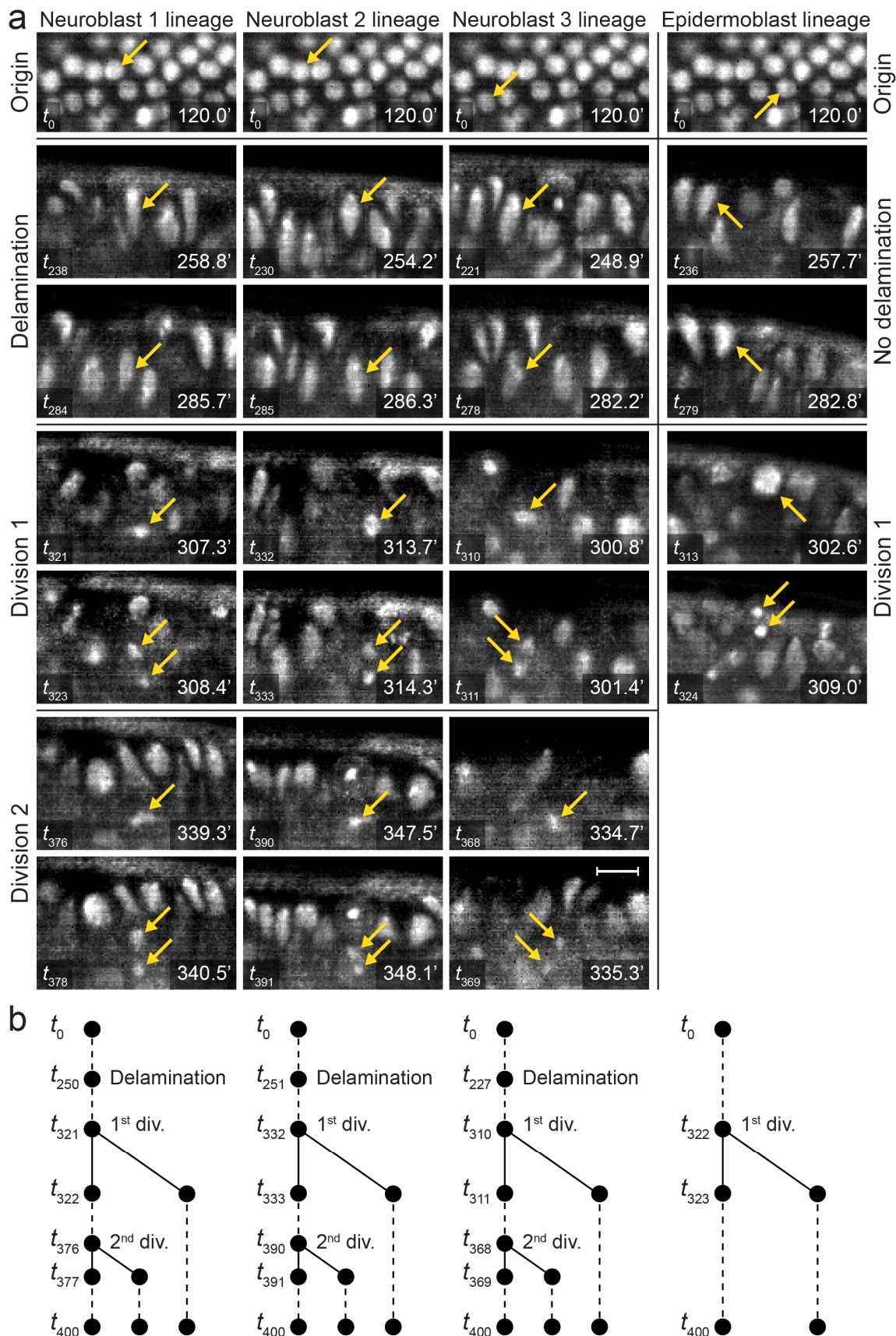
4D manual tracking was performed for a period of 113 time points in the two-photon SiMView recording presented in **Supplementary Video 5**, using the ImageJ Manual Tracking plug-in (<http://rsbweb.nih.gov/ij/plugins/track/track.html>). The spatial tracking coordinates were converted into a Vaa3D-compatible data format and rendered using Vaa3D version 2.7 (Peng *et al.*, *Nature Biotechnology*, 2011). This figure shows an example of a manually reconstructed cell track with a total length of approximately 250  $\mu\text{m}$ , superimposed with maximum-intensity projections of the fused SiMView data set. Note that the two-dimensional Vaa3D visualization highlights the rendered track on top of the maximum-intensity projection and thus gives the impression of a superficial trajectory. The three-dimensional cell location, however, is in a non-superficial layer of the germ band throughout the analyzed time window (optical depth between 32.5  $\mu\text{m}$  at  $t_0$  and 44.7  $\mu\text{m}$  at  $t_{112}$ ).

(a) Maximum-intensity projection of the two-photon SiMView recording at time point  $t_6$ , superimposed with the rendered track between  $t_0$  and  $t_6$ .

(b) Maximum-intensity projection of the two-photon SiMView recording at time point  $t_{56}$ , superimposed with the rendered track between  $t_0$  and  $t_{56}$ .

(c) Maximum-intensity projection of the two-photon SiMView recording at time point  $t_{112}$ , superimposed with the rendered track between  $t_0$  and  $t_{112}$ .

Supplementary Figure 10 | Reconstruction of neuroblast and epidermoblast lineages



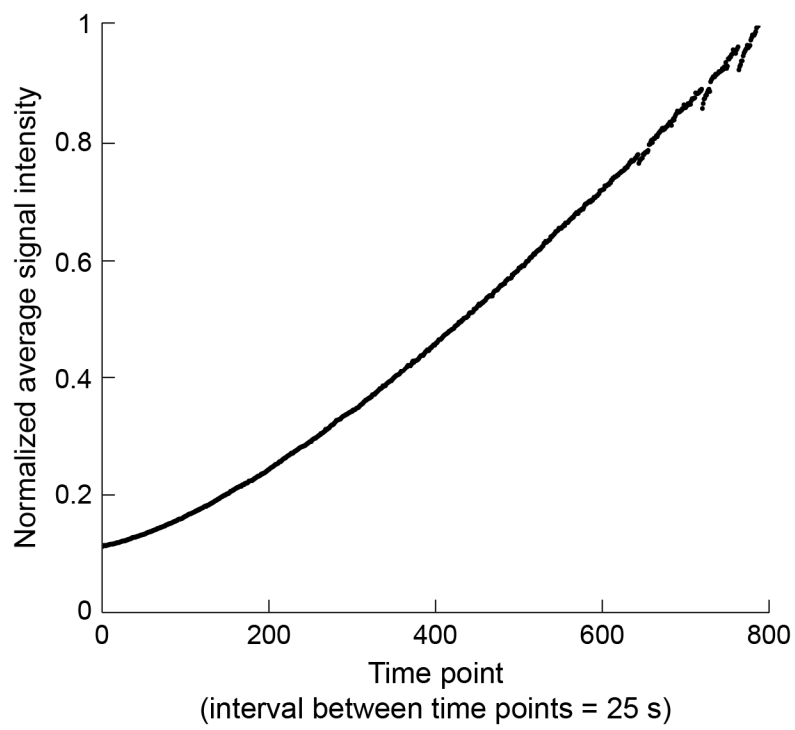
## Supplementary Figure 10 | Reconstruction of neuroblast and epidermoblast lineages

(a) Raw optical slices from SiMView recording in **Supplementary Video 3** for key events in the lineage reconstructions visualized in **Fig. 6a,b** and **Supplementary Video 11**. Optical slices indicate blastoderm origins, delamination, first cell division and second cell division for three neuroblasts, as well as blastoderm origin and first cell division for one epidermoblast. Yellow arrows indicate the locations of the nuclei of the tracked cells. The appearance of stripes in the raw data arises from the column gain variability typically encountered in first generation sCMOS cameras (such as the Andor Neo detector used in this recording). The SiMView processing pipeline contains a module for measuring column gain factors and correcting these stripes.

(b) Lineage trees for the neuroblast/epidermoblast lineage reconstructions visualized in **Fig. 6a,b** and **Supplementary Video 11** (1<sup>st</sup> div. = first division, 2<sup>nd</sup> div. = second division). Four blastoderm cells and their respective daughter cells were manually tracked from time point 0 to 400 (120-353 minutes post fertilization, 35 second temporal resolution), using Imaris (Bitplane) and ImageJ (<http://rsbweb.nih.gov/ij/>). Tracks start in the blastoderm (time point 0). The neuroblasts delaminate between time points 227 and 251, and subsequently produce ganglion mother cells in two division cycles (first cycle between time points 310 and 332, second cycle between time points 368 and 390). The epidermoblast remains in the outer cell layer and divides once at time point 313. Manual tracking was performed until time point 400 for all cells.

Scale bar, 10  $\mu\text{m}$ .

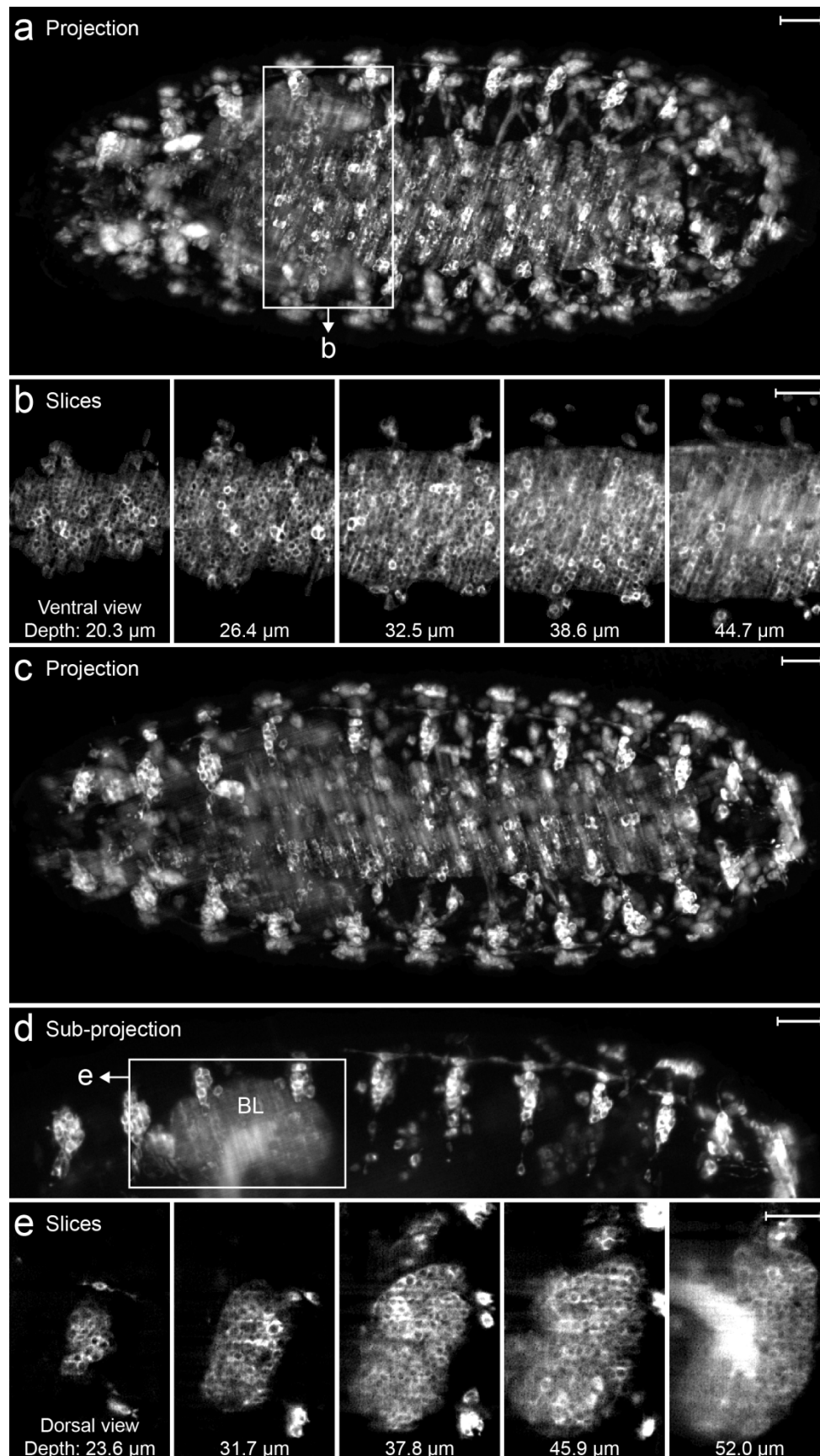
**Supplementary Figure 11** | Time-course of *C155-GAL4,UAS-mCD8::eGFP* signal intensity



**Supplementary Figure 11** | Time-course of *C155-GAL4,UAS-mCD8::eGFP* signal intensity

The figure shows the time course of average GFP signal intensity in a high-speed live recording of the developing nervous system (**Supplementary Video 13**). Simultaneous multi-view imaging started shortly after the onset of GFP expression at around 9.5 hours post fertilization (time point 0). Approximately 400,000 images of the developing nervous system were recorded over the period 9.5-15 hours post fertilization. Despite continuous high-speed image acquisition, GFP signal intensities were constantly increasing. The fluctuations towards the end of the plot represent signal changes in the percent-range, which arise from re-orientation of the embryo after the onset of global muscle contractions.

Supplementary Figure 12 | SiMView optical slices of the *Drosophila* VNC and brain lobes



**Supplementary Figure 12** | SiMView optical slices of the *Drosophila* VNC and brain lobes

**(a)** Maximum-intensity projection of an image stack from the simultaneous multi-view time-lapse recording of the *Drosophila* embryonic nervous system shown in **Supplementary Video 12** (one-photon SiMView recording at 14.5 hours post fertilization).

**(b)** Optical slices from the image stack visualized in (a) show the part of the ventral nerve cord (VNC) highlighted by the white rectangle. The images demonstrate that one-photon SiMView resolves the cell bodies with an average diameter of 2-3  $\mu\text{m}$  and thus achieves cellular resolution for the majority of the VNC. Images were deconvolved with the Lucy-Richardson algorithm (5 iterations).

**(c)** Maximum-intensity projection of an image stack from the simultaneous multi-view time-lapse recording of the *Drosophila* embryonic nervous system shown in **Supplementary Video 13** (one-photon SiMView imaging at 14.5 hours post fertilization).

**(d)** Sub-stack maximum-intensity projection of the data set visualized in (c), showing one of the brain lobes (BL). The sub-stack covers 1/3 of the z-range of the complete stack and comprises the entire brain lobe.

**(e)** Optical slices from the image stack visualized in (c) and (d) show the brain lobe highlighted by the white rectangle in (d). The images demonstrate that one-photon SiMView resolves cell bodies and thus achieves cellular resolution for a large fraction of the brain lobe. Images were deconvolved with the Lucy-Richardson algorithm (5 iterations).

Scale bars, 25  $\mu\text{m}$ .

**Supplementary Table 1** | Components of the one-photon SiMView light sheet microscope

Module	Component	Product(s)	Manufacturer
Lasers (shared modules)	SOLE-6 module	Solid-state lasers: 488/642/685 nm DPSS lasers: 515/561/594 nm	Omicron Laserage
	SOLE-3 module	Solid-state lasers: 405/445 nm	Omicron Laserage
Illumination sub-systems (two mirrored modules)	High-speed laser shutter	VS14S2ZM1-100 with AlMgF2 coating VMM-D3 three-channel driver	Uniblitz
	Illumination filter wheel	96A351 filter wheel MAC6000 DC servo controller	Ludl
		NDQ neutral density filters	Melles Griot
	Miniature piezo tip/tilt mirror	S-334 tip/tip mirror E-503.00S amplifier E-509.S3 servo controller E-500 chassis	Physik Instrumente
		F-theta lens	S4LFT4375
	Tube lens module	U-TLU-1-2 camera tube	Olympus
	Piezo objective positioner	P-725 piezo E-665 piezo amplifier and servo controller	Physik Instrumente
	Illumination objective	XLFLUOR 4x/340/0.28	Olympus
Detection sub-systems (two mirrored modules)	Piezo objective positioner	P-725 piezo E-665 piezo amplifier and servo controller	Physik Instrumente
	Detection objective	CFI60/75 LWD water-dipping series	Nikon
		Apochromat/Plan-Apochromat water-dipping series	Carl Zeiss
	Detection filter wheel	96A354 filter wheel MAC6000 DC servo controller	Ludl
RazorEdge and EdgeBasic long-pass filters BrightLine band-pass filters		Semrock	

**Supplementary Table 1 (continued)**

Module	Component	Product(s)	Manufacturer
Detection sub-systems (two mirrored modules)	Tube lens module	CFI second lens unit	Nikon
		AxioImager 130 mm ISD tube lens	Carl Zeiss
	Camera	Neo sCMOS	Andor/Koolance
		ExosII re-circulator	Hamamatsu
Specimen chamber with perfusion system	Four-view specimen chamber	Scaffold manufactured from black Delrin	Custom design
	Specimen holder	Holder manufactured from medical-grade stainless steel	Custom design
		Multi-stage adapter module for connection to specimen positioning system	
	Perfusion system	REGLO dual-channel 12-roller pump	Harvard Apparatus
Model 107 benchtop environmental chamber		TestEquity	
Specimen positioning system	Customized translation stages (three units)	M-111K046	Physik Instrumente
	Rotary stage	M-116	Physik Instrumente
	Motion I/O interface and amplifier	C-809.40 4-channel servo-amplifier	Physik Instrumente
	Motion controller	PXI-7354 4-axis stepper/servo motion controller	National Instruments
Real-time electronics	Real-time controller with LabVIEW Real-Time OS	PXI-8110 Core 2 Quad 2.2 GHz	National Instruments
	I/O interface boards (three units)	PXI-6733 high-speed analog output 8-channel board	National Instruments
	BNC connector boxes (three units)	BNC-2110 shielded connector block	National Instruments
	Serial interface board	PXI-8432/2	National Instruments

**Supplementary Table 1 (continued)**

Module	Component	Product(s)	Manufacturer
Control software	Real-time modules	32-bit LabVIEW code	Custom software
	Host modules	64-bit LabVIEW code C-compiled Matlab code	Custom software
Workstations and servers	Data acquisition workstation	2x X5680 HexaCore CPUs	Intel Corporation
		18x 8 GB DDR-3 RAM modules	Kingston
		24-channel RAID controller 52445	Adaptec
		24x Cheetah 15K.7 SAS-2 600GB hard disks	Seagate
		10 Gigabit fiber network adapter EXPX9501AFXSR	Intel Corporation
		GeForce GTX470 graphics card	Nvidia Corporation
	Fiber network-attached storage server	2x Neon CameraLink frame grabbers	BitFlow
		2x PCIe-1429 Full-Configuration CameraLink frame grabbers	National Instruments
		X8DAH+-F server board	Supermicro
		S5520SC-based standard rack-mount server	Intel Corporation
Fiber network-attached RAID systems	2x ESDS A24S-G2130 24-disk enclosure	Infortrend	
	48x Ultrastar A7K2000 SATA-2 2TB hard disks	Hitachi	

**Supplementary Table 2** | Components of the two-photon SiMView light sheet microscope

Module	Component	Product(s)	Manufacturer
Lasers (shared modules)	Pulsed IR laser	Chameleon Ultra II	Coherent
	SOLE-3 module	Solid-state lasers: 488/561/594 nm	Omicron Laserage
Illumination sub-systems (two mirrored modules)	Beam attenuation module	AHWP05M-980 mounted achromatic half-wave plate (690-1200 nm) GL10-B Glan-laser polarizer (650-1050 nm)	Thorlabs
	Pockels cell	Model 350-80-LA-02 KD*P series electro-optic modulator Model 302RM driver	Conoptics
	IR beam splitter	PBSH-450-2000-100 broadband polarizing cube beam splitter	Melles Griot
		WPA1312-2-700-1000 achromatic 1/2 wave plate	Casix
	High-speed laser shutter	VS14S2ZM1-100 with AlMgF2 coating VMM-D3 three-channel driver	Uniblitz
	Illumination filter wheel	96A351 filter wheel	Ludl
		MAC6000 DC servo controller	Melles Griot
	Miniature piezo tip/tilt mirror	NDQ neutral density filters	Melles Griot
		S-334 tip/tip mirror E-503.00S amplifier E-509.S3 servo controller E-500 chassis	Physik Instrumente
	F-theta lens	66-S80-30T-488-1100nm custom lens	Special Optics
	Tube lens module	U-TLU-1-2 camera tube	Olympus
Piezo objective positioner	P-622.1CD PIHera piezo linear stage E-665 piezo amplifier and servo controller	Physik Instrumente	
Illumination objective	LMPLN5XIR 5x/0.10	Olympus	
	LMPLN10XIR 10x/0.30		

**Supplementary Table 2 (continued)**

Module	Component	Product(s)	Manufacturer
Detection sub-systems (two mirrored modules)	Piezo objective positioner	P-622.1CD PIHera piezo linear stage E-665 piezo amplifier and servo controller	Physik Instrumente
	Detection objective	CFI60/75 LWD water-dipping series	Nikon
		Apochromat/Plan-Apochromat water-dipping series	Carl Zeiss
	Detection filter wheel	96A354 filter wheel	Ludl
		MAC6000 DC servo controller BrightLine short-pass and band-pass filters	Semrock
	Tube lens module	CFI second lens unit	Nikon
Axiolmager 130 mm ISD tube lens		Carl Zeiss	
Camera	Neo sCMOS ExosII re-circulator	Andor/Koolance	
Specimen chamber with perfusion system	Four-view specimen chamber	Scaffold manufactured from black Delrin	Custom design
	Specimen holder	Holder manufactured from medical-grade stainless steel	Custom design
		Multi-stage adapter module for connection to specimen positioning system	
Perfusion system	REGLO dual-channel 12-roller pump	Harvard Apparatus	
	Model 107 benchtop environmental chamber	TestEquity	
Specimen positioning system	Customized translation stages (three units)	M-111K046	Physik Instrumente
	Rotary stage	M-116	Physik Instrumente
	Motion I/O interface and amplifier	C-809.40 4-channel servo-amplifier	Physik Instrumente
	Motion controller	PXI-7354 4-axis stepper/servo motion controller	National Instruments

**Supplementary Table 2 (continued)**

Module	Component	Product(s)	Manufacturer
Real-time electronics	Real-time controller with LabVIEW Real-Time OS	PXI-8110 Core 2 Quad 2.2 GHz	National Instruments
	I/O interface boards (three units)	PXI-6733 high-speed analog output 8-channel board	National Instruments
	BNC connector boxes (three units)	BNC-2110 shielded connector block	National Instruments
	Serial interface board	PXI-8432/2	National Instruments
Control software	Real-time modules	32-bit LabVIEW code	Custom software
	Host modules	64-bit LabVIEW code C-compiled Matlab code	Custom software
Workstations and servers	Data acquisition workstation	2x X5680 HexaCore CPUs	Intel Corporation
		18x 8 GB DDR-3 RAM modules	Kingston
		24-channel RAID controller 52445	Adaptec
		24x Cheetah 15K.7 SAS-2 600GB hard disks	Seagate
		10 Gigabit fiber network adapter EXPX9501AFXSR	Intel Corporation
		GeForce GTX470 graphics card	Nvidia Corporation
		2x Neon CameraLink frame grabbers	BitFlow
		2x PCIe-1429 Full-Configuration CameraLink frame grabbers	National Instruments
		X8DAH+-F server board	Supermicro
		Fiber network-attached storage server	S5520SC-based standard rack-mount server
Fiber network-attached RAID systems	2x ESDS A24S-G2130 24-disk enclosure	Infortrend	
	48x Ultrastar A7K2000 SATA-2 2TB hard disks	Hitachi	

**Supplementary Table 3** | Specifications of simultaneous multi-view imaging experiments

Experiment	<i>Drosophila</i> syncytial blastoderm (specimen #1)	<i>Drosophila</i> syncytial blastoderm (specimen #2)
Related figures	Figs. 2a-e, 3b,c; 5c Suppl. Fig. 5	Figs. 2f, 5a,b,d,e Suppl. Fig. 6
Related videos	Video 10	Videos 1, 8, 9
Imaging framework	One-photon SiMView	
Excitation wavelength	488 nm	
Illumination objectives	Olympus XLFLUOR 4x/340/0.28	
Detection filters	Semrock RazorEdge LP488 U-grade	
Detection objectives	Carl Zeiss C-Apochromat 10x/0.45 W	Nikon CFI75 LWD 16x/0.8 W
Cameras	Hamamatsu Orca Flash 2.8	Andor Neo sCMOS
Temperature	25.0°C	
Sample embedding	0.4% low-melting temperature agarose in tap water	
Imaging period	1.94 hours 201 time points	1.61 hours 233 time points
Temporal sampling	35 seconds	25 seconds
Recording period per time point	15 seconds	10 seconds
Exposure time	20 milliseconds	25 milliseconds
Voxel size	0.36 x 0.36 x 2.00 $\mu\text{m}^3$	0.41 x 0.41 x 2.03 $\mu\text{m}^3$
Images per time point	4 x 125	4 x 120
Total # of images	100,500	111,840
Size of data set	518 gigabytes	1.12 terabytes
Post-acquisition fusion	5-level Daubechies D4 wavelet fusion	20-pixel linear blending

**Supplementary Table 3 (continued)**

Experiment	<i>Drosophila</i> embryonic development (specimen #1)	<i>Drosophila</i> embryonic development (specimen #2)
Related figures	Fig. 3d	Figs. 3a, 6a Suppl. Figs. 7, 10a
Related videos	Video 2	Videos 3, 11
Imaging framework	One-photon SiMView	
Excitation wavelength	488 nm	
Illumination objectives	Olympus XLFLUOR 4x/340/0.28	
Detection filters	Semrock RazorEdge LP488 U-grade	
Detection objectives	Nikon CFI75 LWD 16x/0.8 W	
Cameras	Andor Neo sCMOS	
Temperature	25.0°C	
Sample embedding	0.4% low-melting temperature agarose in tap water	
Imaging period	17.08 hours 2051 time points	19.44 hours 2001 time points
Temporal sampling	30 seconds	35 seconds
Recording period per time point	15 seconds	
Exposure time	25 milliseconds	
Voxel size	0.41 x 0.41 x 2.03 $\mu\text{m}^3$	
Images per time point	4 x 130	4 x 125
Total # of images	1,066,520	1,000,500
Size of data set	10.73 terabytes	10.06 terabytes
Post-acquisition fusion	20-pixel linear blending	20-pixel linear blending

**Supplementary Table 3** (continued)

Experiment	<i>Drosophila</i> embryonic development (specimen #3)	<i>Drosophila</i> embryonic development (specimen #4)
Related figures	Fig. 4b Suppl. Fig. 9	Fig. 4c
Related videos	Video 5	Video 6
Imaging framework	Two-photon SiMView	
Excitation wavelength	940 nm	
Illumination objectives	Olympus LMPLN10XIR 10x/0.3	
Detection filters	Semrock BrightLine SP680 Semrock BrightLine BP525/50	
Detection objectives	Nikon CFI75 LWD 16x/0.8 W	
Cameras	Andor Neo sCMOS	
Temperature	25.0°C	
Sample embedding	0.4% low-melting temperature agarose in tap water	
Imaging period	1.42 hours 171 time points	2.71 hours 326 time points
Temporal sampling	30 seconds	
Recording period per time point	20 seconds	
Exposure time	150 milliseconds	
Voxel size	0.41 x 0.41 x 2.03 $\mu\text{m}^3$	
Images per time point	2 x 110	2 x 105
Total # of images	37,620	68,460
Size of data set	387 gigabytes	705 gigabytes
Post-acquisition fusion	4-pixel linear blending (axially only)	4-pixel linear blending (axially only)

**Supplementary Table 3 (continued)**

Experiment	<i>Drosophila</i> stage 16 slicing series
Related figures	Fig. 4a
Related videos	Video 4
Imaging framework	Two-photon SiMView
Excitation wavelength	940 nm
Illumination objectives	Olympus LMPLN10XIR 10x/0.3
Detection filters	Semrock BrightLine SP680 Semrock BrightLine BP525/50
Detection objectives	Nikon CFI75 LWD 16x/0.8 W
Cameras	Andor Neo sCMOS
Temperature	25.0°C
Sample embedding	0.4% low-melting temperature agarose in tap water
Imaging period	Single time point
Temporal sampling	–
Recording period per time point	–
Exposure time	200 milliseconds
Voxel size	0.41 x 0.41 x 0.41 $\mu\text{m}^3$
Images per time point	2 x 593
Total # of images	1,186
Size of data set	12 gigabytes
Post-acquisition fusion	3-pixel linear blending (axially only)

**Supplementary Table 3** (continued)

Experiment	<i>Drosophila</i> neural development <i>C155-GAL4</i> (specimen #1)	<i>Drosophila</i> neural development <i>C155-GAL4</i> (specimen #2)
Related figures	Fig. 6c,d Suppl. Figs. 8, 12a,b	Suppl. Figs. 11, 12c-e
Related videos	Videos 7, 12, 15	Videos 13, 14
Imaging framework	One-photon SiMView	
Excitation wavelength	488 nm	
Illumination objectives	Olympus XLFLUOR 4x/340/0.28	
Detection filters	Semrock RazorEdge LP488 U-grade	
Detection objectives	Nikon CFI75 LWD 16x/0.8 W	
Cameras	Andor Neo sCMOS	
Temperature	25.0°C	
Sample embedding	0.4% low-melting temperature agarose in tap water	
Imaging period	5.83 hours 701 time points	5.47 hours 788 time points
Temporal sampling	30 seconds	25 seconds
Recording period per time point	15 seconds	
Exposure time	25 milliseconds	
Voxel size	0.41 x 0.41 x 2.03 $\mu\text{m}^3$	
Images per time point	4 x 140	4 x 130
Total # of images	392,560	409,760
Size of data set	3.95 terabytes	4.12 terabytes
Post-acquisition fusion	20-pixel linear blending	20-pixel linear blending

**Supplementary Table 3** (continued)

Experiment	<i>Drosophila</i> neural development <i>Ftz-ng-GAL4</i> (specimen #1)	<i>Drosophila</i> neural development <i>Ftz-ng-GAL4</i> (specimen #2)	<i>Drosophila</i> neural development <i>Ftz-ng-GAL4</i> (specimen #3)
Related figures	Fig. 6e	–	–
Related videos	Videos 16, 17, 19	Video 18	Video 20
Imaging framework	One-photon SiMView		
Excitation wavelength	488 nm		
Illumination objectives	Olympus XLFLUOR 4x/340/0.28		
Detection filters	Semrock RazorEdge LP488 U-grade		
Detection objectives	Carl Zeiss Plan-Apochromat 40x/1.0 W		
Cameras	Andor Neo sCMOS		
Temperature	25.0°C		
Sample embedding	0.4% low-melting temperature agarose in tap water		
Imaging period	1.37 hours 165 time points	8.33 hours 1,001 time points	2.13 hours 256 time points
Temporal sampling	30 seconds		
Recording period per time point	15 seconds		
Exposure time	25 milliseconds		
Voxel size	0.16 x 0.16 x 2.03 $\mu\text{m}^3$		
Images per time point	4 x 110	4 x 115	4 x 105
Total # of images	72,600	460,460	107,520
Size of data set	748 gigabytes	4.63 terabytes	1.08 terabytes
Post-acquisition fusion	20-pixel linear blending	20-pixel linear blending	20-pixel linear blending